The Zero-Density Limit of the Residual Entropy Scaling of Transport Properties

Ian H. Bell,[*,†] Robert Hellmann,[‡,¶] and Allan H. Harvey[†]

†*Applied Chemicals and Materials Division, National Institute of Standards and Technology, Boulder, CO 80305*

‡*Institut für Chemie, Universität Rostock, 18059 Rostock, Germany*

¶*Present Address: Institut für Thermodynamik, Helmut-Schmidt-Universität/Universität der Bundeswehr Hamburg, 22043 Hamburg, Germany*

E-mail: ian.bell@nist.gov

Abstract

The modified residual entropy scaling approach has been shown to be a successful means of scaling dense phase transport properties. In this work, we investigate the dilute-gas limit of this scaling. This limit is considered for model potentials and highly accurate results from calculations with ab initio pair potentials for small molecules. These results demonstrate that with this approach, the scaled transport properties of noble gases can be collapsed without any empirical parameters to nearly their mutual uncertainties and that the scaled transport properties of polyatomic molecules are qualitatively similar, and for sufficiently high temperatures they agree with "universal" values proposed by Rosenfeld in 1999. There are significant quantitative differences between the model potentials and real fluids in these scaled coordinates, but this study provides a thorough coverage of model fluids and simple real fluids, providing the basis for further study. In the supporting information we provide the collected calculations with ab initio pair potentials from the literature, as well as code in the Python language implementing all aspects of our analysis.

1 Introduction

In 1977, Rosenfeld[1] proposed that the macroscopically-reduced transport properties in the liquid phase ought to be uniquely specified by their residual entropy (sometimes called "excess entropy", which is misleading because that term has a different meaning in chemical thermodynamics). The macroscopically reduced transport properties are defined by[2]

$$\widetilde{\lambda} \equiv \frac{\lambda}{k_{\mathrm{B}}\rho_{\mathrm{N}}^{2/3}\sqrt{k_{\mathrm{B}}T/m}} \tag{1}$$

$$\widetilde{\eta} \equiv \frac{\eta}{\rho_{\mathrm{N}}^{2/3}\sqrt{mk_{\mathrm{B}}T}} \tag{2}$$

$$\widetilde{D} \equiv \frac{\rho_{\mathrm{N}}^{1/3}D}{\sqrt{k_{\mathrm{B}}T/m}} \tag{3}$$

where λ is the thermal conductivity, η is the viscosity, D is the self-diffusion coefficient, ρ_{N} is the number density in particles per volume, m is the mass of one particle, k_{B} is Boltzmann's constant, and T is the absolute temperature.

For the model potentials, reduced (starred) units are used, which results in the identical definitions for the macroscopically reduced transport properties of

$$\widetilde{\lambda} = \frac{\lambda^*}{(\rho^*)^{2/3}\sqrt{T^*}} \tag{4}$$

$$\widetilde{\eta} = \frac{\eta^*}{(\rho^*)^{2/3}\sqrt{T^*}} \tag{5}$$

$$\widetilde{D} = \frac{(\rho^*)^{1/3}D^*}{\sqrt{T^*}} = \frac{(\rho^* D^*)}{(\rho^*)^{2/3}\sqrt{T^*}} \tag{6}$$

where $\lambda^* = \lambda\sigma^2/(k_\mathrm{B}\sqrt{\varepsilon/m})$, $D^* = D/(\sigma\sqrt{\varepsilon/m})$, $\eta^* = \eta\sigma^2/\sqrt{m\varepsilon}$, $\rho^* = \rho_\mathrm{N}\sigma^3$, $T^* = k_\mathrm{B}T/\varepsilon$, and $\rho^* D^* = (\rho_\mathrm{N}D)\cdot(\sigma^2/\sqrt{\varepsilon/m})$. The variable ε is the energy scaling parameter, and σ is the length scaling parameter.

In 1999, Rosenfeld[3] noted that for dilute gases of finite density the macroscopically-reduced transport properties should be proportional to the residual entropy to the power of 2/3, based on a study of inverse power law potentials. An empirical scaling approach that satisfies the necessary behavior in the liquid phase[1] and the gas phase[3] is to multiply the macroscopically-reduced transport properties by the residual entropy to the power of 2/3, and use this scaling throughout the entire fluid domain. This approach was first proposed by Bell,[4] and subsequently applied to the Lennard-Jones 12-6 fluid.[2] Thus the +-scaled transport properties are given by

$$\eta^+ \equiv \widetilde{\eta}\cdot(-s^\mathrm{r}/k_\mathrm{B})^{2/3} \tag{7}$$

$$\lambda^+ \equiv \widetilde{\lambda}\cdot(-s^\mathrm{r}/k_\mathrm{B})^{2/3} \tag{8}$$

$$D^+ \equiv \widetilde{D}\cdot(-s^\mathrm{r}/k_\mathrm{B})^{2/3} \tag{9}$$

These scaled transport properties have the characteristic that they are well-conditioned in the zero-density limit (our focus in this work) and do not diverge at zero density like the scaled coordinates of Eqs. (1) to (3). Additionally, the +-scaled transport properties also demonstrate a nearly monovariate dependence on the residual entropy $-s^\mathrm{r}/k_\mathrm{B}$ from the low-density gas into the deeply supercooled liquid for nonassociating fluids.

As derived in Bell et al.,[2] in the zero-density limit, these +-scaled transport properties can be rewritten in terms of second virial coefficients B_2, and given as

$$\lim_{\rho_\mathrm{N}\to 0}\eta^+ = \frac{\eta_{\rho_\mathrm{N}\to 0}}{\sqrt{mk_\mathrm{B}T}}\left[T\left(\frac{\mathrm{d}B_2}{\mathrm{d}T}\right)+B_2\right]^{2/3} \tag{10}$$

$$\lim_{\rho_\mathrm{N}\to 0}\lambda^+ = \frac{\lambda_{\rho_\mathrm{N}\to 0}}{k_\mathrm{B}\sqrt{k_\mathrm{B}T/m}}\left[T\left(\frac{\mathrm{d}B_2}{\mathrm{d}T}\right)+B_2\right]^{2/3} \tag{11}$$

$$\lim_{\rho_\mathrm{N}\to 0}D^+ = \frac{(\rho_\mathrm{N}D)_{\rho_\mathrm{N}\to 0}}{\sqrt{k_\mathrm{B}T/m}}\left[T\left(\frac{\mathrm{d}B_2}{\mathrm{d}T}\right)+B_2\right]^{2/3} \tag{12}$$

or in reduced (starred) units

$$\lim_{\rho_\mathrm{N}\to 0}\eta^+ = \frac{\eta^*_{\rho_\mathrm{N}\to 0}}{\sqrt{T^*}}\left[T^*\left(\frac{\mathrm{d}B_2^*}{\mathrm{d}T^*}\right)+B_2^*\right]^{2/3} \tag{13}$$

$$\lim_{\rho_\mathrm{N}\to 0}\lambda^+ = \frac{\lambda^*_{\rho_\mathrm{N}\to 0}}{\sqrt{T^*}}\left[T^*\left(\frac{\mathrm{d}B_2^*}{\mathrm{d}T^*}\right)+B_2^*\right]^{2/3} \tag{14}$$

$$\lim_{\rho_\mathrm{N}\to 0}D^+ = \frac{(\rho^* D^*)_{\rho_\mathrm{N}\to 0}}{\sqrt{T^*}}\left[T^*\left(\frac{\mathrm{d}B_2^*}{\mathrm{d}T^*}\right)+B_2^*\right]^{2/3} \tag{15}$$

in which $B_2^* = B_2/\sigma^3$.

The scaling proposed here has some similarities with that of the hard sphere scaling, an approach (along with its empirical modifications) that has seen extensive study in the past decades. The review of Silva and Liu[5] provides an extensive discussion of how the hard sphere scaling of transport properties has been applied to a range of molecular systems.

The exponent on the residual entropy of 2/3, obtained from a consideration of dilute particles modeled with inverse power law potentials,[2,3] does not currently have any broader significance in entropy scaling. Mode-coupling theory predicts that the shear viscosity should be proportional to the shear rate to the power of 3/2, though recent simulations have called that exponent into question.[6] There remain many unanswered questions in the field of entropy scaling of transport properties, so a connection between shear rate and residual entropy could exist, but it is not self-evident.

The term $\left[T\left(\frac{\mathrm{d}B_2}{\mathrm{d}T}\right)+B_2\right]^{2/3}$ corresponds to an effective cross-sectional area of the molecule[5] which monotonically decreases with the temperature (see Fig. 6). In the Modified Enskog theory[7] (see also Section 9.3.2 of Ref. 5), the effective second virial coefficient $T\left(\frac{\mathrm{d}B_2}{\mathrm{d}T}\right)+B_2$ is used within the Enskog theory for hard spheres, and is obtained by replacing the pressure for the hard sphere by the thermal pressure of the real fluid (where the thermal pressure is defined by $T(\partial p/\partial T)_\rho$).

In order to calculate the +-scaled transport properties in the zero-density limit, it is necessary to be able to evaluate the transport properties (η, λ, $\rho_\mathrm{N}D$), the second virial coefficient B_2, and the temperature derivative of B_2. Equivalently, reduced (starred) units can be employed.

Applying the term residual entropy scaling to the zero-density limit is a misnomer because the residual entropy is by definition always zero at zero density. Nonetheless, the scaling we investigate in this work flows directly from the discoveries made in the modeling of the transport properties of dense phases from residual entropy scaling.

The primary focus of this work is to investigate the behavior of these scaled transport properties in the limit of zero density for a range of different types of interactions between molecules. In Section 2 we consider model pair potentials from fully repulsive (inverse power law, hard sphere, and EXP), to pair potentials with repulsion and attraction (Mie, EXP-6), and potentials with attraction, repulsion and dipolar interactions (Stockmayer). In Section 3 we consider the results from highly accurate ab initio calculations for noble gases and small polyatomic molecules. The overarching theme is to identify similarities and differences between the model potentials and real fluids in this new scaling framework for zero-density limit transport properties.

2 Model Potentials

The model potentials discussed in this section are relatively simple, spherically symmetric pair interactions. These simple models, while they do not fully capture the interactions between molecules, are commonly used to probe the physics of real substances.

2.1 Second Virial Coefficients

For spherically symmetric pair interactions with a potential V that is uniquely a function of distance r, the second virial coefficient B_2 can be expressed by the integral

$$B_2 = 2\pi\int_0^\infty \left[1-\exp\left(-\frac{V(r)}{k_\mathrm{B}T}\right)\right]r^2\mathrm{d}r \quad (16)$$

For more complex pair potentials (e.g., the Stockmayer potential), Eq. (16) is generalized so that the integrand at each value of r is averaged over all mutual orientations of the two molecules.

For simple model potentials, it is common[8–10] that the result of the integration is a closed-form infinite summation. Variable-numerical-precision libraries exist that can be used to calculate B_2 to any desired level of accuracy. Temperature derivatives of B_2 can be obtained by taking the temperature derivative of the integrand of Eq. (16) and performing a similar numerical integration. Where closed-form solutions for B_2 exist, they are used, and complex step derivatives[11,12] are used to evaluate the temperature derivative of the closed-form solutions. Direct numerical evaluation of Eq. (16) can be useful to verify an implementation's correctness.

Equation (16) assumes classical mechanics; for real fluids (especially those of low mass and/or moment of inertia, and especially at low temperatures) quantum effects are significant. It is usually adequate to include quantum corrections by a first-order approach that replaces $V(r)$ in Eq. (16) by an "effective" potential depending on the gradients of the potential and the related reduced mass and torques. In this work, no quantum effects were applied to the model potentials. Values of B_2 for the more realistic ab initio potentials considered in Section 3 typically employed at least first-order quantum corrections; in some cases (as explained in the cited papers) more complete accounting of quantum effects was performed.

In this work we have chosen to non-dimensionalize the temperature by the Boyle temperature of the fluid instead of its critical temperature. In the zero-density limit, the critical region has only an incidental connection to the nature of the fluid, while the Boyle temperature is much more meaningful. The Boyle temperature corresponds to the temperature at which the second virial coefficient is equal to zero; i.e., the temperature at which the first derivative of the compressibility factor Z with respect to density is zero. Physically, this temperature can be interpreted as the temperature at which the attractive and repulsive forces in the low-density gas phase are perfectly balanced *on average*. The Boyle temperature is connected to the critical temperature because in the end, all properties are manifestations of the interactions between molecules. This connection is the origin of approaches like that of Tsonopoulos[13] to obtain generalized forms for the virial coefficients (and therefore, Boyle temperatures) based on the critical point of the fluid.

2.2 Transport Properties

In the first-order approximation, the transport properties are given as

$$[\eta_{\rho_{\rm N}\to 0}]_1 = \frac{5}{16\sigma^2}\left(\frac{mk_{\rm B}T}{\pi}\right)^{1/2}\frac{1}{\Omega^{(2,2)*}} \tag{17}$$

$$[\lambda_{\rho_{\rm N}\to 0}]_1 = \frac{75}{64\sigma^2}\left(\frac{k_{\rm B}^3T}{m\pi}\right)^{1/2}\frac{1}{\Omega^{(2,2)*}} \tag{18}$$

$$[(\rho_{\rm N}D)_{\rho_{\rm N}\to 0}]_1 = \frac{3}{8\sigma^2}\left(\frac{k_{\rm B}T}{m\pi}\right)^{1/2}\frac{1}{\Omega^{(1,1)*}} \tag{19}$$

or in starred units

$$[\eta^*_{\rho_{\rm N}\to 0}]_1 = \frac{5}{16\sqrt{\pi}}\frac{\sqrt{T^*}}{\Omega^{(2,2)*}} \tag{20}$$

$$[\lambda^*_{\rho_{\rm N}\to 0}]_1 = \frac{15}{4}[\eta^*_{\rho_{\rm N}\to 0}]_1 \tag{21}$$

$$[(\rho^* D^*)_{\rho_{\rm N}\to 0}]_1 = \frac{3\sqrt{T^*}}{8\sqrt{\pi}\Omega^{(1,1)*}} \tag{22}$$

Higher-order Sonine corrections are available for some but not all of the model potentials, and as a result, we have decided to consistently use the first-order approximation for all model potentials.

The collision integrals $\Omega^{(1,1)*}$ and $\Omega^{(2,2)*}$ must be obtained by numerical approaches for all but the simplest fully repulsive potentials. For each of the model potentials described, the literature source employed for the collision integral is described. Usually the collision integrals are tabulated, and then interpolation is used to obtain the value of the collision integral at intermediate values. The transport property effective area ($\sigma^2\Omega^{(2,2)*}$ for η and λ, and $\sigma^2\Omega^{(1,1)*}$ for D) monotonically decreases with increasing temperature (see Fig. 6) in an analogous fashion to that of the virial coefficient effective area. At high temperatures, the ratio of these effective area terms is nearly constant, which is why the +-scaled transport properties approximately approach a horizontal asymptote.

The collision integrals appearing in the above equations are usually calculated with the assumption of classical mechanics, although a complete quantum calculation is possible for spherically symmetric potentials. In Section 3, we use quantum-calculated collision integrals for helium and neon, and classical values for all other molecules. Unfortunately, in contrast to the calculation of B_2, no viable approach has been developed to apply quantum corrections to transport collision integrals; this introduces an unknown but probably small amount of inconsistency in our analyses in Section 3.

2.3 Fully Repulsive Potentials

Fully repulsive potentials are those for which $V(r) > 0$ and $\mathrm{d}V/\mathrm{d}r \leq 0$ at all values of r. Their thermodynamic behavior is simplified because they do not have a vapor-liquid phase transition. Their second virial coefficients are always positive, because $V(r) > 0$ means that the integrand in Eq. (16) is positive. Here we consider the inverse-power-law (IPL), hard-sphere, and EXP potentials.

The inverse-power-law (IPL) potential is given by

$$V(r) = \varepsilon \left(\frac{\sigma}{r}\right)^n \tag{23}$$

in which V is the potential in units of energy, ε is the energy scaling parameter, r is the distance between particles, σ is the length scaling parameter (not to be confused with the diameter), and n is the "hardness" of the potential, all parameters being positive. The EXP potential is given by

$$V(r) = \phi_0 \exp(-r/\sigma) \tag{24}$$

in which ϕ_0 is the energy scaling parameter, r is the distance between particles, and σ is the length scaling parameter.

In the +-scaled coordinates described above, the transport properties of the IPL potential have no temperature dependence because the temperature dependence of the collision integral is perfectly canceled by the temperature dependence of the virial coefficient contribution. The values for η^+, λ^+, and D^+ are given by numerical integrations, and tabulated values (and the requisite code in Python to evaluate them) are available in the SI of Bell et al.[2]

The zero-density properties of the EXP potential were studied in the 1950s and 1960s, and evaluation of its virial coefficients and convergent series expansions approximations to its virial coefficients are available in Sherwood and Mason[14] and Henderson and Oden.[15] Values of the collision integrals $\Omega^{(1,1)*}$ and $\Omega^{(2,2)*}$ are provided in Monchick[17] in tabular form and are interpolated to calculate the transport properties of the EXP potential. Section 1.1 in the SI summarizes the necessary mathematics to evaluate these models for the EXP potential. The length scale parameter of the EXP potential cancels, leaving ϕ_0/k_B as the temperature scaling parameter. Even so, there is only a single curve for the EXP potential capturing all values of ϕ_0/k_B.

In Fig. 1 we show the scaled viscosity and self-diffusion coefficient for a range of IPL potentials and the EXP potential. The hard sphere case is the limiting value ($n \to \infty$) of the IPL potential.

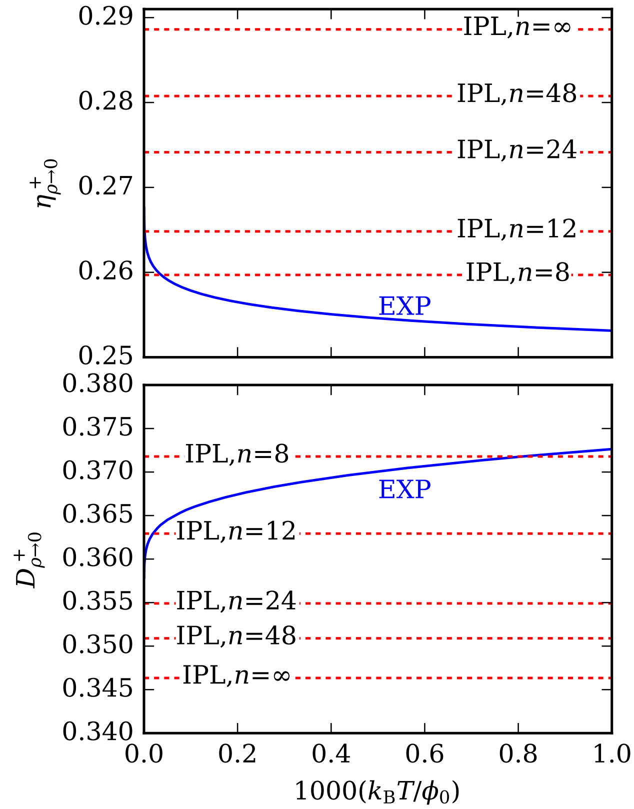

Figure 1: Scaled viscosity and self-diffusion coefficient for IPL potentials of hardness n, the hard sphere (IPL with $n = \infty$), and the EXP potential.

2.4 Mie Potential

Pair potentials that include the effects of attraction and repulsion more faithfully represent the properties of real fluids. The Mie family is formed as a scaled difference of two IPL potentials in which both of the IPL exponents n and m are adjustable parameters:

$$V(r) = C\varepsilon \left[\left(\frac{\sigma}{r}\right)^n - \left(\frac{\sigma}{r}\right)^m\right] \tag{25}$$

with

$$C = \left(\frac{n}{n-m}\right)\left(\frac{n}{m}\right)^{m/(n-m)} \tag{26}$$

The Mie potential contains the well-known Lennard-Jones 12–6 potential (a Mie potential with $n = 12$ and $m = 6$). The exponent 6 of the Lennard-Jones 12–6 potential can be derived from theory,[18,19] while the repulsive exponent n is usually an empirical parameter.

The B_2^* of the n–6 Mie potential (see Eq. (25)) is obtained from the closed-form infinite series solution of Sadus,[8,9] truncated at 200 terms, and the temperature derivative of B_2^* is obtained by complex step derivatives. A similar formulation for B_2^* was available as far back as the year 1924.[20] The collision integrals for the n–6 Mie potentials are obtained from the empirical correlation of Fokin et al.[21] (In the work of Fokin et al. it should be $\ln(m)$ rather than $\ln(1/m)$ in Eq. 4b).

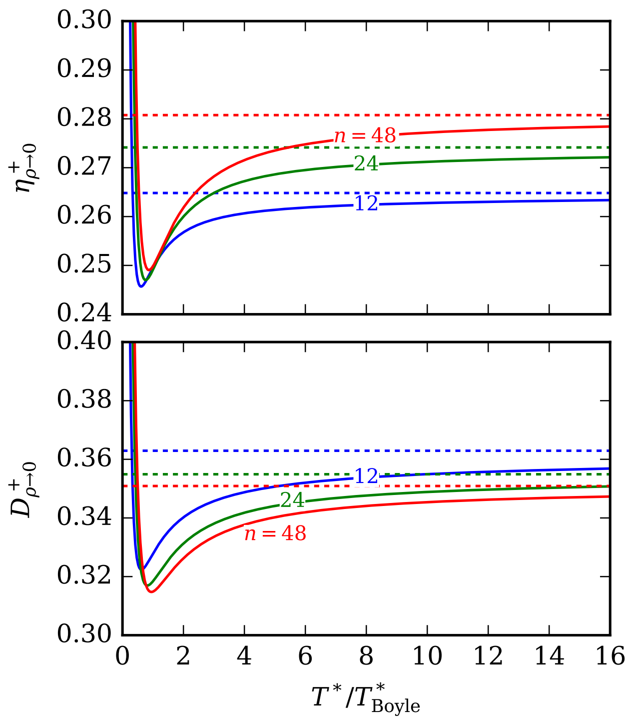

Figure 2: Scaled viscosity and self-diffusion coefficient for Mie n–6 potentials in the first-order approximation for the transport properties. The dashed line for each Mie potential corresponds to the value for the IPL potential of hardness n; this is the infinite temperature limit for each Mie potential.

Figure 2 shows η^+ and D^+ in the zero-density limit. The Mie potential has both attraction and repulsion and therefore the Boyle temperature can be calculated, and the temperatures for each potential are scaled by their Boyle temperature. These results demonstrate that changing the repulsive exponent of the Mie potential has only a relatively modest impact on the +–scaled transport properties. The relative change in the value of the +-scaled properties at high temperatures is intimately linked to the relative change in the IPL potential values of hardness n because they are the high-temperature limits of the respective n–6 Mie potential. The minimum value of the potential only shifts by a small amount.

The +-scaled transport properties of the Mie potential approach a constant value at high temperatures; this is unlike the behavior for real substances. In the case of noble gases, as temperature is increased, they approach the high-temperature behavior of the EXP potential rather than the behavior of an IPL potential of fixed hardness (see Fig. 7). Another way of saying this is that the *effective* Mie exponent changes as a function of temperature for real fluids at high temperatures. The Mie potential itself (see Ref. 8, Fig. 2) bears a qualitative resemblance to the scaled transport properties shown in Fig. 2. While intriguing, we cannot think of any deeper physical significance to this similarity.

2.5 EXP-6 Potential

It is known that the Mie potentials are not the ideal model for the repulsive part of the pair potential; an exponential function is more suitable. The generalized EXP-6 potential has the r^{-6} attractive term along with an exponential repulsive term.

The EXP-6 potential[22,23] is given by

$$V(r) = \frac{\varepsilon}{1-\frac{6}{\alpha}}\left[\frac{6}{\alpha}\exp\left(\alpha\left(1-\frac{r}{r_{\mathrm{m}}}\right)\right) - \left(\frac{r_{\mathrm{m}}}{r}\right)^6\right] \tag{27}$$

in which ε is the energy scaling parameter, α is the scalar parameter controlling the repulsion of the potential, r is the distance between particles, and r_m is the separation at which the potential is at its minimum. When the attractive part of the potential is neglected (or when its influence becomes negligible at very high temperatures), the EXP-6 potential reduces to an EXP potential.

The B_2^* values are obtained from tabulated values from Rice and Hirschfelder,[22] and collision integrals were taken from Mason[23] in tabular form. A brief description of the mathematics required for the EXP-6 results is provided in the SI (Section 1.2).

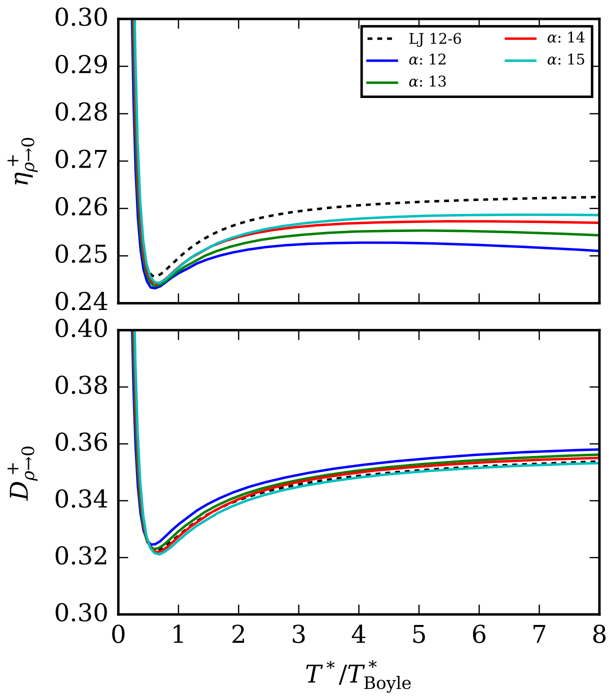

Figure 3: Scaled viscosity and self-diffusion coefficient in the first-order approximation for EXP-6 potentials and the Lennard-Jones 12-6 potential.

Figure 3 shows the scaled transport properties for the EXP-6 potential for a range of hardnesses α. Just like real noble gases, the values of η^+ do not approach a constant value at high temperature, and their high-temperature limit is the EXP potential (an EXP-6 potential without the r^{-6} attractive term). The values of D^+ on the other hand are very similar and also similar to those of the Lennard-Jones 12-6 potential.

2.6 Stockmayer Potential

The classical 12-6-3 Stockmayer pair potential is the Mie 12-6 potential with the subtraction of an orientation-dependent point dipole contribution,

$$V(r,\theta_1,\theta_2,\phi) = 4\varepsilon\left[\left(\frac{\sigma}{r}\right)^{12} - \left(\frac{\sigma}{r}\right)^{6}\right] - V_\mu \quad (28)$$

where

$$\frac{V_\mu}{\varepsilon(\mu^*)^2\left(\dfrac{\sigma}{r}\right)^3} = [2\cos\theta_1\cos\theta_2 - \sin\theta_1\sin\theta_2\cos\phi] \quad (29)$$

The reduced dipole moment, expressed in *Système International* units, is

$$(\mu^*)^2 = \frac{\mu^2}{4\pi\epsilon_0\varepsilon\sigma^3}, \quad (30)$$

in which μ is in C·m, σ is in m, ε is in J, ϵ_0 is the vacuum permittivity (also known as the electric constant), with the value of $8.8541878128 \times 10^{-12}$ C^2·N^{-1}·m^{-2} (see ref. 24, an updated value from that of ref. 25).

For the virial coefficient, we use the closed form solution of Bartke and Hentschke,[26] with additional terms in the series expansion as described in the SI (Section 1.3). Other closed-form implementations can be found in the literature,[27–30] but it was not possible to evaluate these models due to typographical errors and/or insufficient description. Tabulated values of B^* are available in Hirschfelder et al.[32] for verification purposes.

The evaluation of B_2^* from the formulation of Bartke and Hentschke[26] requires a significant amount of computational effort due to the large number of indefinite integrals required. In order to save computational time, Chebyshev expansions of degree 100 of $(T^*\mathrm{d}B_2^*/\mathrm{d}T^* + B_2^*)^{2/3}$ as a function of T^* were constructed with the `ChebTools` library[33] and evaluated to obtain the virial coefficient contribution. One expansion was constructed for each of the values of $(\mu^*)^2$ included in Monchick and Mason.[34]

For the transport properties, Monchick and Mason[34] tabulated values of the collision integrals $\Omega^{(2,2)*}$ and $\Omega^{(1,1)*}$ for selected values of $(\mu^*)^2$, from which the transport properties can be evaluated by interpolation of the collision integrals. It should be noted that Monchick and Mason obtained their values for the collision integrals in an approximate manner. First, they calculated values for the collision integrals for fixed angular orientations of the particles in the same way as for particles interacting through a spherically-symmetric potential. Then, they averaged the collision integrals over the angular orientations. This approximation (commonly known as the "Mason–Monchick approximation") corresponds to the unphysical assumption that the relative orientations of the two particles do not change during the collision process. An accurate treatment of the collision dynamics would, however, result in transport property values that also depend on the reduced moments of inertia of the particles.

Figure 4 shows the scaled transport properties for the Stockmayer potential. As the reduced dipole moment $(\mu^*)^2$ is increased, the deviations from the LJ 12-6 potential increase, and the limit of zero dipole moment is the LJ 12-6 potential itself. The inclusion of the point-dipole shifts the zero-density transport properties much more significantly than the relatively minor modifications to the repulsive part of the EXP-6 or Mie potentials. The variation within the family of Stockmayer potentials of reduced dipole moments $(\mu^*)^2$ approximates the behaviors of small polar molecules. In addition, while the Stockmayer potential with reduced dipole moment $(\mu^*)^2$ of zero (the LJ 12-6 potential) demonstrates minima for viscosity and self-diffusion at a value of $T/T_{\mathrm{Boyle}} \approx 0.5$, as the dipole moment is increased, the minima disappear. The disappearance of the minima of the scaled transport properties for fluids with greater polarity is consistent with the behavior seen below (see Section 3) for fluids with somewhat polar interactions.

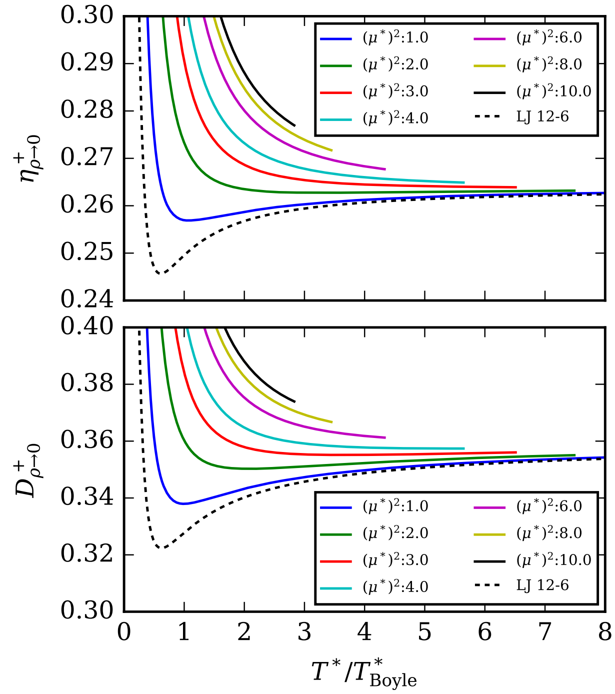

Figure 4: Scaled viscosity and self-diffusion coefficient in the first-order approximation for 12-6-3 Stockmayer potentials of reduced dipole moment $(\mu^*)^2$ and the Lennard-Jones 12-6 potential.

3 Ab Initio Pair Potentials

The intermolecular interactions of real fluids are more complicated than the "toy" potentials described above. Therefore, extensive efforts have been invested, particularly in the last decade, to model the zero-density transport properties and virial coefficients of real fluids from first principles.

The potential energy surface between a pair of molecules is a function of distance and orientation. Points on the surface are generated by computing the energy of the pair and subtracting the energies of the isolated monomers. Attainment of high accuracy requires the use of large basis sets and of ab initio methods that account for electron correlation at a high level (such as CCSD(T), coupled-cluster singles and doubles with perturbative triples contribution).[35] With present computing capabilities, such high-accuracy calculations are only tractable for pairs where each molecule has roughly three (or fewer) "heavy" atoms, where in this context a heavy atom is anything with more than two electrons. Typically, thousands of ab initio points are generated for each pair, and then these points are fitted to a suitable function (with attention to necessary boundary conditions at large and small distances) in order to enable calculation of virial coefficients and collision integrals.

The ab initio potentials are almost always developed under the assumption that the molecules are rigid, although for a few systems (such as H_2O and D_2O)[36] virial coefficients have been calculated that incorporate intramolecular vibration. Molecules with internal conformational degrees of freedom, such as normal alkanes larger than propane, add enough additional complication that high-accuracy ab initio potential energy surfaces are not currently available; even if they were available the evaluation of collision integrals for such molecules is currently intractable. We therefore restrict our work here to molecules that can be treated as rigid to a good approximation.

3.1 Second Virial Coefficients

The second virial coefficients can be very accurately calculated numerically from ab initio potentials and are usually tabulated at a range of temperatures. With the exception of ^{4}He,[38] the temperature derivatives of the virial coefficients were not made available directly in the respective study. Calculating very accurate smoothed values of the virial coefficients between tabulated values of temperature is a surprisingly challenging endeavor, not well suited to conventional interpolation techniques.

Therefore, we used an optimization approach to fit nonlinear correlation functions to the ab initio results for B_2; one example of this approach is that of Harvey and Lemmon for ordinary water.[70] We utilized a similar nonlinear functional form, given by

$$\frac{B_2}{B_{2,\mathrm{scale}}} = \sum_{i=1}^{N} c_i (T_{\mathrm{scale}}/T)^{t_i} \tag{31}$$

where the number of terms N was determined to suit the given fluid, T_{scale} is a parameter used to scale the temperature, and $B_{2,\mathrm{scale}}$ is a parameter used to scale the second virial coefficient. With this functional form, the temperature derivative term is equal to

$$T\left(\frac{\mathrm{d}B_2}{\mathrm{d}T}\right) = B_{2,\mathrm{scale}} T \left(\frac{\mathrm{d}B_2}{\mathrm{d}\left(\frac{T_{\mathrm{scale}}}{T}\right)}\right)\left(\frac{\mathrm{d}\left(\frac{T_{\mathrm{scale}}}{T}\right)}{\mathrm{d}T}\right) \tag{32}$$

$$= -B_{2,\mathrm{scale}} \sum_{i=1}^{N} c_i t_i \left(\frac{T_{\mathrm{scale}}}{T}\right)^{t_i} \tag{33}$$

We carried out a hybrid optimization scheme to obtain the correlations for the second virial coefficients. The exponents t_i were optimized in an outer evolutionary optimization loop, constrained to be in the range (0.2, 20). For each set of exponents t_i, a linear-least-squares fit was carried out to obtain the best set of coefficients c_i. In this manner, reliable and accurate second virial coefficients were obtained for all the ab initio results. The goal was to reproduce the second virial coefficient within 0.1% except for in the vicinity of the Boyle temperature. The second virial coefficient correlations obtained and statistics about the goodness of fit are presented in the SI (Section 2.2). We also provide the Python script used to fit the correlations.

3.2 Noble Gases

The noble gases represent the simplest “molecules”. They are spherically symmetric and form the basis of a significant body of molecular modeling efforts. It has long been proposed that corresponding states should apply to the noble gases, and as such, the pair potentials should map onto each other with the appropriate selection of the temperature scaling parameter $\varepsilon/k_{\mathrm{B}}$ and the length scaling parameter σ.

3.2.1 Transport Properties

Figure 5a presents the scaled transport properties obtained from ab initio calculations for the noble gases as well as the respective deviations from the corresponding values for xenon. With *zero* adjustable scaling parameters, the viscos-

Table 1: The references for the virial coefficients, constant volume specific heat correlations, and transport properties employed in this work as obtained from ab initio calculations. The chemical formulas are given in Hill System Order, and the molecules are sorted by molar mass. The critical temperature T_{crit} is obtained from the reference equation of state used to obtain $c_{v,0}$ and the Boyle temperature T_{Boyle} is obtained by interpolation of the ab initio results for B_2. An entry of "TW" indicates that the values are presented in this work in the SI, and the associated potential energy surface is indicated by the reference.

Formula	Name	M / g·mol^{-1}	T_{crit} / K	T_{Boyle} / K	$c_v^{(0)}$	B_2	η	λ	ρD
^4He	helium-4	4.0026	5.2	23.2	37	38	38	38	N.A.
CH_4	methane	16.0428	190.6	511.4	39	40	41	42	41
H_2O	ordinary water	18.0153	647.1	1410.9	43	36	44	45	TW[46,47]
OD_2	heavy water	20.0275	643.8	1395.9	48	36	49	49	49
Ne	neon	20.1790	44.4	119.5	50	51	51	51	N.A.
N_2	nitrogen	28.0135	126.2	325.9	52	TW[a]	53	53	TW[53]
C_2H_6	ethane	30.0690	305.3	759.5	54	55	55	55	55
H_2S	hydrogen sulfide	34.0809	373.1	944.9	56	57	57	45	57
Ar	argon	39.9480	150.7	408.6	58	59	59	59	60
CO_2	carbon dioxide	44.0098	304.1	714.3	61	62	62	62	TW[62]
N_2O	nitrous oxide	44.0128	309.5	769.5	56	63	63	63	63
C_2H_4O	ethylene oxide	44.0526	468.9	1129.2	64	65	65	65	65
C_3H_8	propane	44.0956	369.9	881.8	66	67	67	67	67
Kr	krypton	83.7980	209.5	574.9	56	68	68	68	68
Xe	xenon	131.2930	289.7	794.9	56	69	69	69	69

a: The nitrogen B_2 values differ from those of the original publication[53] because the treatment of quantum effects has changed. The treatment of quantum effects for the new values is similar to that applied for CO_2.[62]

ity, thermal conductivity, and self-diffusion coefficient values of argon, krypton, and xenon agree within their mutual uncertainty over nearly the complete temperature range. The +-scaled standard uncertainty is approximately 0.1-0.4% for krypton (the noble gases are all similar) for all three transport properties (see the SI, Section 2.1). Thus the expanded ($k = 2$ coverage factor) uncertainty for one noble gas would be 0.2-0.8%, and their mutual uncertainty band would be 0.4-1.6%. The effect of molecular size is removed because the impact of molecular size on the transport property and the virial coefficient contribution effectively cancel. The curves are not entirely coincident, and especially at lower Boyle-reduced temperatures, the deviations increase. The gases with non-negligible quantum effects (neon and helium-4) represent increasing deviations from the behavior of xenon. When neon and helium-4 are treated classically, they too fall back into alignment with the higher noble gases.

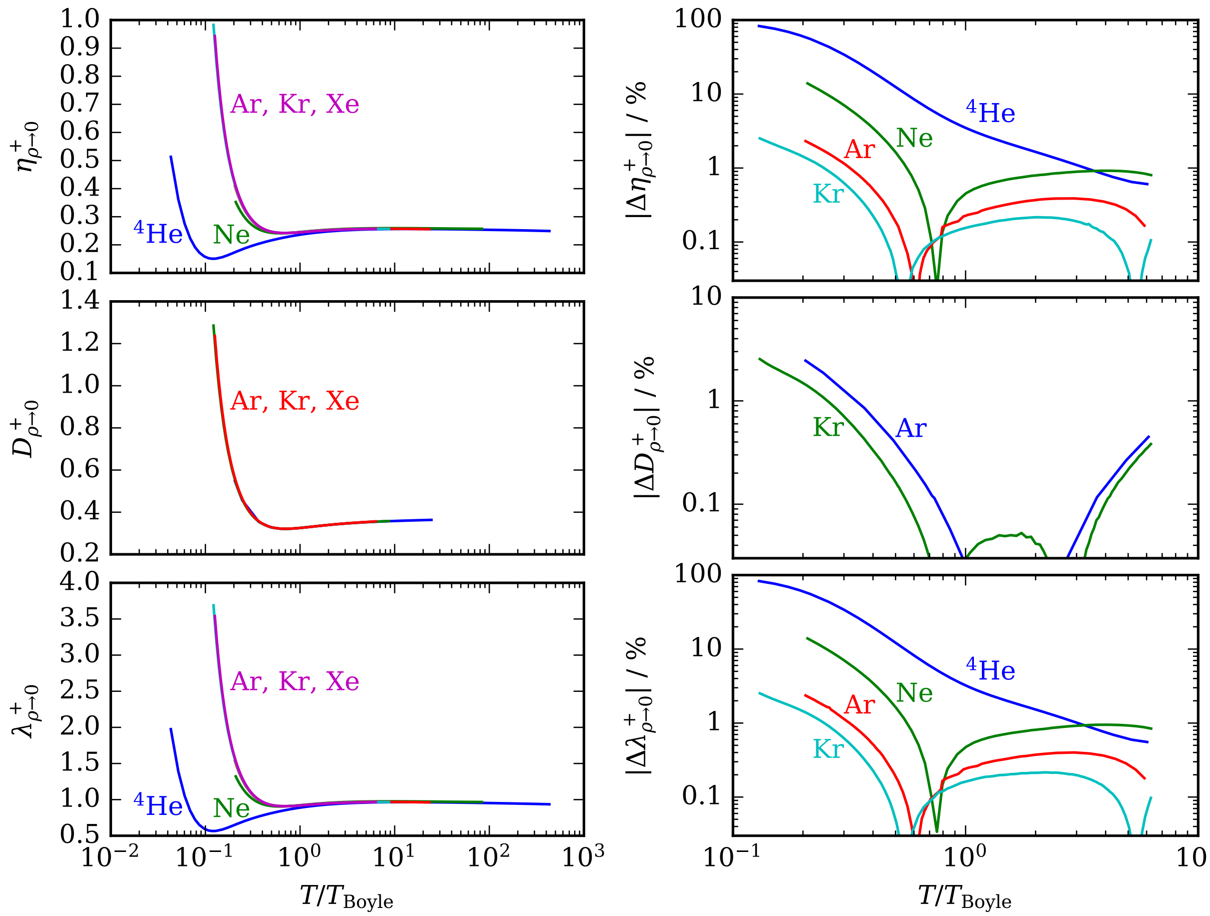

(a) The +-scaled transport properties.

(b) Percentage deviation from the respective value for xenon. The deviation term for property Y is defined by $\Delta Y = 100 \times (Y/Y_{\text{Xe}} - 1)$. The deviations can only be evaluated for values of T/T_{Boyle} that are available for both the gas and Xe.

Figure 5: Scaled transport properties for noble gases ^{4}He, Ne, Ar, Kr, and Xe.

As discussed above, the effective area from the transport properties and the effective area from the virial coefficients are approximately proportional to each other, especially at higher temperatures. Figure 6 shows that for viscosity both of the effective areas are of similar magnitude, and as temperature increases, their ratio becomes approximately constant. This is the origin of the nearly horizontal asymptote for $\eta_{\rho_{\rm N}\to 0}$ in Fig. 5a, though at higher temperatures, the curves do begin to curl downwards and approach the EXP potential (see the next section).

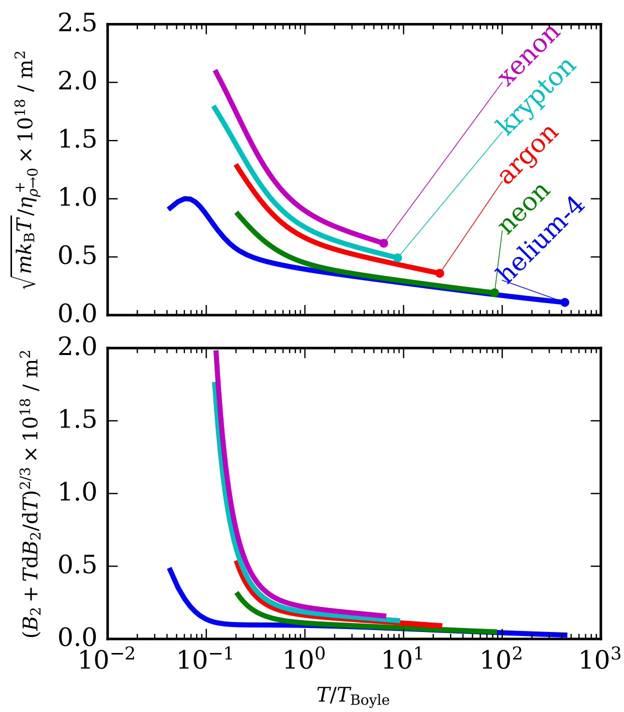

Figure 6: Effective areas involved in the +-scaled viscosity for the noble gases.

3.2.2 High-Temperature Limit

For each of the noble gases without strong quantum effects, an exponential function of the form of Eq. (24) was fit directly to the potential at the smallest inter-particle distances, and from that the leading coefficient $\phi_0/k_{\rm B}$ was obtained. Figure 7 shows the +-scaled viscosities of the noble gases along with the EXP potential plotted as a function of the temperature scaled by $\phi_0/k_{\rm B}$. Although there is some variation due to the fitting of $\phi_0/k_{\rm B}$, the asymptotic behavior of the ab initio potentials is to approach the EXP potential. A similar approach has also been used in the literature for modeling the high-temperature limiting dilute transport properties of noble gases[71] and polyatomic gases.[72,73]

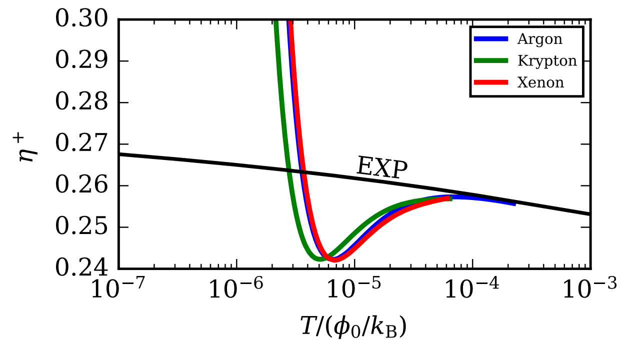

Figure 7: High-temperature limiting behavior of the noble gases as compared with the EXP potential; the value of $\phi_0/k_{\rm B}$ is in the SI (Table S17).

3.3 Molecules

Polyatomic molecules represent more complex transport mechanisms due to their internal degrees of freedom (rotational and vibrational) and the much more complex collision dynamics as a result of the anisotropy of the intermolecular potential and the possibility of inelastic collisions.

3.3.1 Viscosity and Self-Diffusion

Figure 8 presents the scaled transport properties calculated from ab initio potentials in combination with the classical kinetic theory of molecular gases. From a qualitative standpoint, the +-scaled self-diffusion coefficient and viscosity values are rather similar for all fluids. Rosenfeld[3] proposed a universal value for the dilute gas of finite density of $\eta^+ = 0.27 \pm 0.027$ based on a consideration of IPL potentials from hardness $n = 4$ to $n = \infty$, which is not far from the mark, except for at $T/T_{\rm Boyle} < 0.5$, at which point the molecular interactions are strongly influenced by the attraction between molecules. Similarly, for the self-diffusion coefficient, Rosenfeld's proposed value[3] of $D^+ =$

0.37 ± 0.0555 provides significant predictive power except at temperatures $T/T_{\mathrm{Boyle}} < 0.5$. The relative similarity of the values for η^+ and D^+ among the polyatomic fluids demonstrates that the addition of intramolecular degrees of freedom does not have a very significant impact on the respective scaled transport property. As demonstrated above for the noble gases, simply changing the molecular size without changing the nature of the molecule (consider the *n*-alkane series methane, ethane, propane) does not result in a significant change to the scaled values.

The deviations in scaled transport properties between the molecules and the respective value for nitrogen are within 10% for $T/T_{\mathrm{Boyle}} > 1$ for all but H_2O and D_2O. Analogously to the noble gases, the deviations at lower temperatures for $\eta+$ and D^+ increase rather significantly at lower temperatures as the attractive interactions begin to play a larger role.

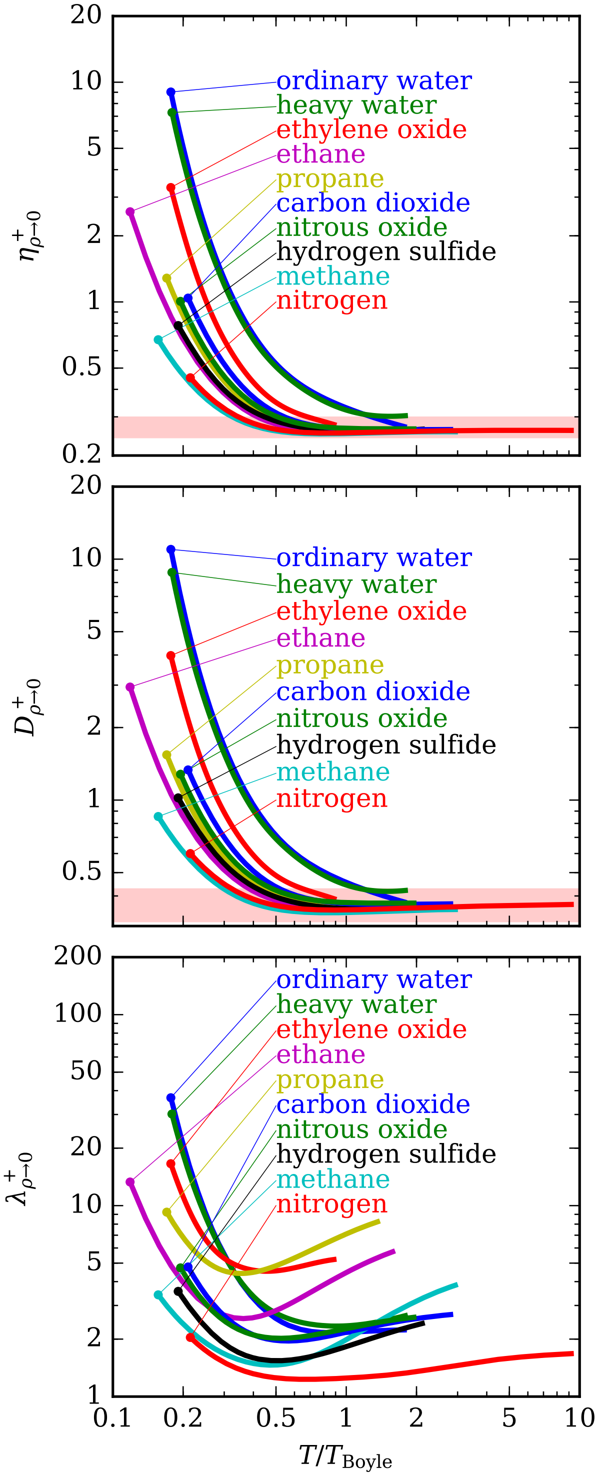

(a) Scaled transport properties. The shaded area corresponds to the respective range of the property proposed by Rosenfeld.[3]

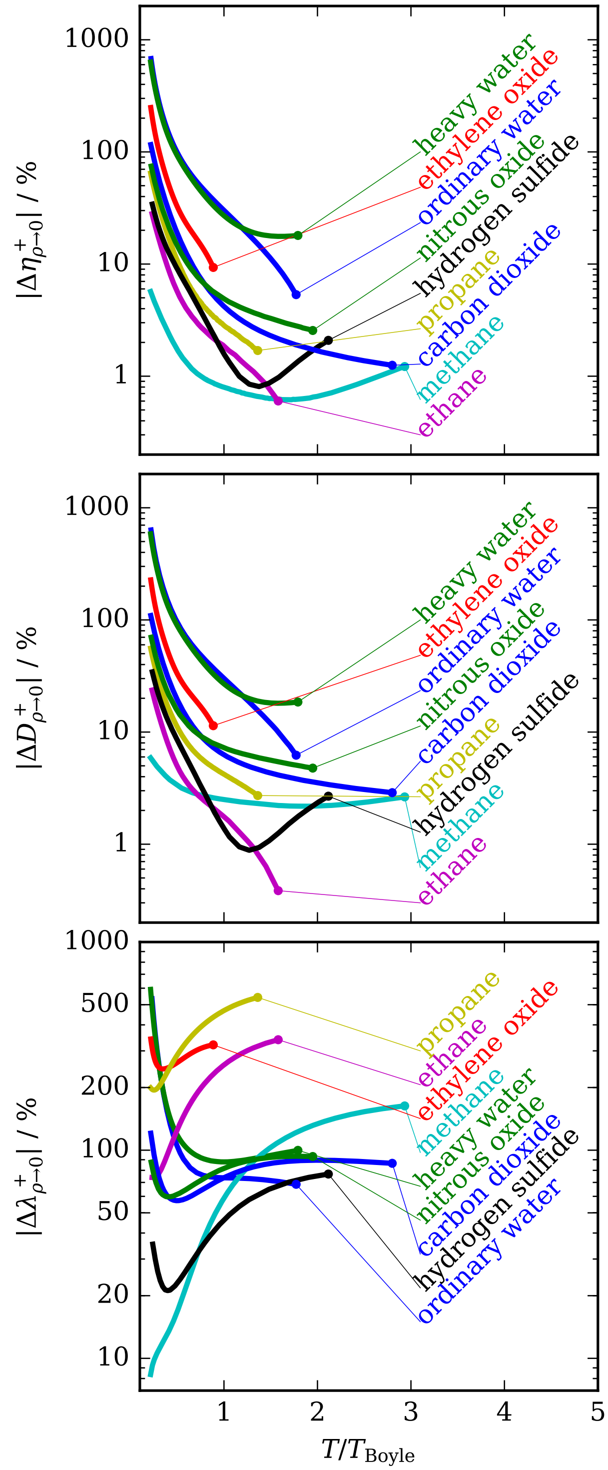

(b) Percentage deviation from the respective value for N_2. The deviation term for property Y is defined by $\Delta Y = 100 \times (Y/Y_{N_2} - 1)$. The deviations can only be evaluated for values of T/T_{Boyle} that are available for both the gas and N_2.

Figure 8: Scaled transport properties for diatomic and polyatomic molecules.

3.3.2 Thermal Conductivity

The story is rather different for the thermal conductivity. Figure 8 also shows the values for the thermal conductivity for the polyatomic molecules. Intramolecular degrees of freedom (DOF) have a much more significant impact on λ^+ than for D^+ or η^+. Thus, the kinetic theory for monatomic gases, which does not account for internal DOF at all, usually fails spectacularly for molecular gases. However, the kinetic theory of molecular gases (used to obtain the values shown in Fig. 8) is too complicated for routine applications, as it requires accurate anisotropic potentials, which became available only in the last two decades. In addition, accurate approaches to treat the vibrational DOF were also found only quite recently (see Hellmann and Bich[45] and references therein). Therefore, typically researchers have resorted to empirical or semi-empirical treatments of the impact of the internal DOF on the thermal conductivity for polyatomic molecules.

In the modified Eucken approach,[45,74] the total thermal conductivity λ is given as the sum of a contribution from translational modes, and another from all grouped internal DOF (rotational and vibrational),

$$\lambda = \lambda_{\text{tr}} + \lambda_{\text{int}} \tag{34}$$

The +-scaled thermal conductivity can be obtained from Eq. (11). A semi-theoretical treatment of λ_{int} is needed because the values of λ for polyatomic molecules vary significantly. On the other hand, when λ_{int} is subtracted off, the pseudo-translational contribution is more similar among polyatomic molecules, as we will show below. As far back as the 1960s it was already shown that the translational and internal thermal conductivity contributions cannot be straightforwardly decoupled in this manner,[45,75] but, to our knowledge, better theoretically-grounded approaches do not exist within the ill-suited framework of the kinetic theory of monatomic gases.

Despite its limitations, we follow the modified Eucken approach, in which the translational contribution λ_{tr} (in W·m^{-1}·K^{-1}) is evaluated from

$$\lambda_{\text{tr}} = \eta f_{\text{tr}} c_{v,\text{tr}}^{(0)} \tag{35}$$

where the viscosity η is in Pa·s, $f_{\text{tr}} = 5/2$, and the translational contribution to the zero-density specific heat $c_{v,\text{tr}}^{(0)}$ is equal to $\frac{3}{2}\frac{R}{M}$ for all molecules, with R the universal gas constant in J·mol^{-1}·K^{-1} and M the molar mass in kg·mol^{-1}.

The contribution to λ from internal DOF (λ_{int}) is given by

$$\lambda_{\text{int}} = \eta \left(\frac{\rho_{\text{mass}} D_{\text{self}}}{\eta}\right) c_{\text{int}}^{(0)} \tag{36}$$

where the product $\rho_{\text{mass}} D_{\text{self}}$ is in Pa·s, and $c_{\text{int}}^{(0)}$ is the specific heat contribution from internal DOF, in J·kg^{-1}·K^{-1}. The value of the mass-specific internal heat capacity $c_{\text{int}}^{(0)}$ is given by

$$c_{\text{int}}^{(0)} = c_v^{(0)} - c_{v,\text{tr}}^{(0)} \tag{37}$$

where $c_v^{(0)}$ is the constant volume specific heat on a mass basis, evaluated from the reference equation of state.

In this work we have values for $\rho_{\text{mass}} D_{\text{self}}$ and η from ab initio calculations, and we use them directly in Eq. (36). On the other hand, the value of $\rho_{\text{mass}} D_{\text{self}}$ is frequently unknown, and it is common to make the assumption of $f_{\text{int}} \equiv \rho_{\text{mass}} D_{\text{self}}/\eta \approx 1.32$. Figure 9 shows the values of $\rho_{\text{mass}} D_{\text{self}}/\eta$ for all fluids from their respective ab initio calculations, expanding on a similar figure from Bich et al.[76] The constant value of 1.32 is far from being a universally applicable recommendation, but it does provide a reasonable representation of the noble gases for $T/T_{\text{Boyle}} < 1$. To that end, we have developed an empirical treatment of f_{int} in which it is a linear function of $\ln(T/T_{\text{Boyle}})$ for $T/T_{\text{Boyle}} \leq 0.4$, and equal to a constant value of 1.39 otherwise. This empirical fit more faithfully represents the values of $\rho_{\text{mass}} D_{\text{self}}/\eta$ from the ab initio calculations for the molecular gases.

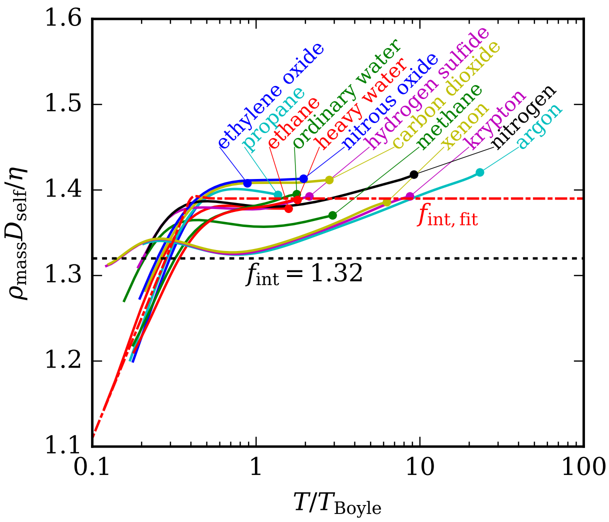

Figure 9: An overlay of the values of $\rho_{\mathrm{mass}} D_{\mathrm{self}}/\eta$ from ab initio calculations.

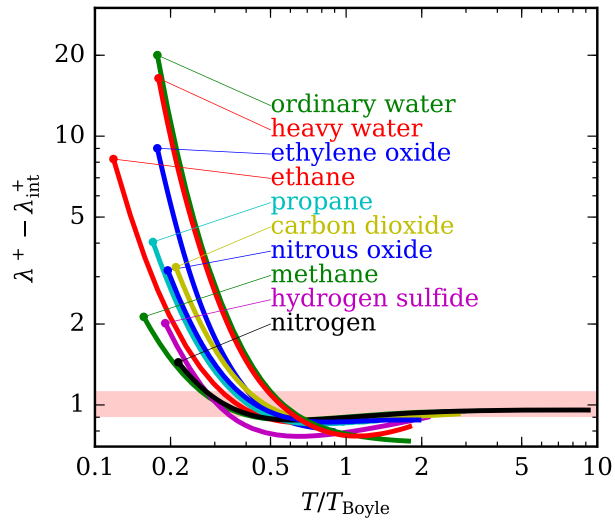

Figure 10: The pseudo-translational contribution to λ^+ for di- and polyatomic molecules. The shaded area represents the band of values proposed by Rosenfeld based on a study of IPL potentials.

Figure 10 shows the pseudo-translational contribution to λ^+ obtained by taking the value of λ^+ from ab initio calculations and subtracting the contribution from the modified Eucken correction. In general, the modified Eucken correction over-corrects the thermal conductivity, which can be seen by comparison with the "universal" value of $\lambda^+ \approx 1.0125 \pm 0.10125$ ($15/4$ times the value for η^+) proposed by Rosenfeld,[3] but the qualitative behavior of the pseudo-translational contribution mirrors the other transport properties considered here.

Nonetheless, the modified Eucken correction remains an imperfect treatment of internal DOF. Even with inclusion of the highly accurate ab initio calculations for $\rho_{\mathrm{mass}} D_{\mathrm{self}}$ and η, the pseudo-translational contribution to λ^+ (theoretically equal to $15\eta^+/4$) does not equal $15\eta^+/4$. Figure 11 shows the relative difference between the pseudo-translational contribution and the value of $15\eta^+/4$. The deviations roughly increase as the polarity of the molecules increases; the relative impacts of molecular size are less pronounced (consider the n-alkane family of methane, ethane, propane).

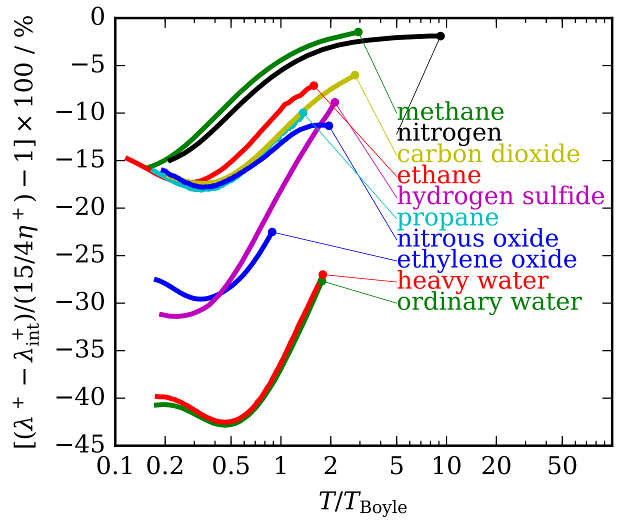

Figure 11: The percentage deviation between the pseudo-translational contribution to λ^+ obtained from the modified Eucken correction and the translational contribution calculated from the viscosity.

4 Conclusions

In this work we have demonstrated that the zero-density limit of the transport properties obtained from modified residual entropy scaling yields a novel approach for scaling of transport properties for model potentials, noble gases, and small di- and polyatomic molecules. The model potentials serve as useful explorations of the scaling approach, and while they do not capture all the physics of larger molecules, they can be used to inform the behavior of real molecules.

For the noble gases with insignificant quantum contributions, the residual entropy scaling leads to a scaling for the zero-density limit that results in a collapse of the scaled transport property data without any empirical scaling parameters. For the polyatomic molecules for which ab initio calculations are possible, the scaled values for self-diffusion coefficient and viscosity show a striking similarity, while the values of the thermal conductivity scatter significantly due to the influence of internal degrees of freedom. Even when a modified Eucken correction is applied to remove the contributions of internal degrees of freedom in an approximate manner, the scaled thermal conductivity values do not collapse as tightly as the other scaled transport properties.

The limitations of computation and theory conspire to restrict the range of molecules that can be modeled by ab initio methods. For now, we must resort to empirical models and the heterogeneous coverage of experimental data that are available in order to model larger molecules of technical relevance. While this is an important topic of research, it is outside the scope of the current study and we must leave it to future work.

We have based our analysis on highly accurate data combined with theoretically-grounded approaches and avoided empiricism as much as possible. Nevertheless, some elements of the analysis could be modified to improve quantitative consistency between fluids. For instance, the selection of the Boyle temperate as the temperature scaling parameter was a subjective choice; the temperature scale could be modified in order to make the low-temperature collapse of fluids more quantitative by fitting a reducing temperature for each fluid, as is commonly done with the Lennard-Jones 12–6 potential.

Supporting Information Available

In order to ensure reproducibility of our results, we have provided in the supporting information: a) the Python code used for each of the model potentials b) the full set of thermophysical property data collected from the literature from ab initio calculations in comma-separated-value form with a consistent unit system c) the empirical fits we obtained for the virial coefficients d) additional description of our methodology that was not appropriate to put in the main manuscript.

Acknowledgement The authors thank: Eric Lemmon (of NIST) for assistance with fitting of virial coefficients, Bradley Alpert (of NIST) for calculating additional coefficients from the Stockmayer expansions, and Arno Laesecke (formerly of NIST) for highlighting the importance of the Stockmayer potential.

Literature Cited

(1) Rosenfeld, Y. Relation between the transport coefficients and the internal entropy of simple systems. *Phys. Rev. A* **1977**, *15*, 2545–2549, DOI: 10.1103/PhysRevA.15.2545.

(2) Bell, I. H.; Messerly, R.; Thol, M.; Costigliola, L.; Dyre, J. Modified Entropy Scaling of the Transport Properties of the Lennard-Jones Fluid. *J. Phys. Chem. B* **2019**, DOI: 10.1021/acs.jpcb.9b05808.

(3) Rosenfeld, Y. A quasi-universal scaling law for atomic transport in simple fluids. *J. Phys.: Condens. Matter* **1999**, *11*, 5415–5427, DOI: 10.1088/0953-8984/11/28/303.

(4) Bell, I. H. Probing the link between residual entropy and viscosity of molecular fluids and model potentials. *Proc. Natl. Acad. Sci. U.S.A.* **2019**, *116*, 4070–4079, DOI: 10.1073/pnas.1815943116.

(5) Silva, C. M.; Liu, H. *Theory and Simulation of Hard-Sphere Fluids and Related Systems*; Springer-Verlag, 2008; Chapter Modelling of Transport Properties of Hard Sphere Fluids and Related Systems, and its Application, pp 383–492, DOI: 10.1007/978-3-540-78767-9_9.

(6) Ge, J.; Todd, B. D.; Wu, G.; Sadus, R. J. Scaling behavior for the pressure and energy of shearing fluids. *Phys. Rev. E* **2003**, *67*, 061201, DOI: 10.1103/physreve.67.061201.

(7) Hanley, H. J. M.; McCarty, R. D.; Cohen, E. G. D. Analysis of the transport coefficients for simple dense fluid: Application of the modified Enskog theory. *Physica* **1972**, *60*, 322–356, DOI: 10.1016/0031-8914(72)90108-5.

(8) Sadus, R. J. Second virial coefficient properties of the n-m Lennard-Jones/Mie potential. *J. Chem. Phys.* **2018**, *149*, 074504, DOI: 10.1063/1.5041320.

(9) Sadus, R. J. Erratum: "Second virial coefficient properties of the n-m Lennard-Jones/Mie potential" [J. Chem. Phys. 149, 074504 (2018)]. *J. Chem. Phys.* **2019**, *150*, 079902, DOI: 10.1063/1.5091043.

(10) Sherwood, A. E.; Mason, E. A. Virial Coefficients for the Exponential Repulsive Potential. *Phys. Fluids* **1965**, *8*, 1577–1579, DOI: 10.1063/1.1761466.

(11) Squire, W.; Trapp, G. Using Complex Variables to Estimate Derivatives of Real Functions. *SIAM Review* **1998**, *40*, 110–112, DOI: 10.1137/s003614459631241x.

(12) Higham, N. Differentiation With(out) a Difference. 2018 (accessed June 1, 2018); https://sinews.siam.org/Details-Page/differentiation-without-a-difference.

(13) Tsonopoulos, C. An empirical correlation of second virial coefficients. *AIChE Journal* **1974**, *20*, 263–272, DOI: 10.1002/aic.690200209.

(14) Ref. 10, Eq. 9.

(15) Henderson, D.; Oden, L. Asymptotic Formulas for the Virial Coefficients using the Exponential Repulsive Potential. *Phys. Fluids* **1966**, *9*, 1592–1594, DOI: 10.1063/1.1761898.

(16) Monchick, L. Collision Integrals for the Exponential Repulsive Potential. *Phys. Fluids* **1959**, *2*, 695–700, DOI: 10.1063/1.1705974.

(17) Ref. 16, Eq. 21.

(18) Eisenschitz, R.; London, F. Über das Verhältnis der van der Waalsschen Kräfte zu den homöopolaren Bindungskräften. *Z. Physik* **1930**, *60*, 491–527, DOI: 10.1007/bf01341258.

(19) London, F. The general theory of molecular forces. *Trans. Faraday Soc.* **1937**, *33*, 8–26, DOI: 10.1039/tf937330008b.

(20) Jones, J. E. On the Determination of Molecular Fields. II. From the Equation of State of a Gas. *Proc. R. Soc. London, Ser. A* **1924**, *106*, 463–477, DOI: 10.1098/rspa.1924.0082.

(21) Fokin, L.; Popov, V.; Kalashnikov, A. Analytical Representation of the Collision Integrals for the (m-6) Lennard-Jones Potentials in the EPIDIF Database. *High Temperatures, Translated from Teplofizika Vysokikh Temperatur* **1999**, *1*, 49–55.

(22) Rice, W. E.; Hirschfelder, J. O. Second Virial Coefficients of Gases Obeying a Modified Buckingham (Exp—Six) Potential. *J. Chem. Phys.* **1954**, *22*, 187–192, DOI: 10.1063/1.1740027.

(23) Mason, E. A. Transport Properties of Gases Obeying a Modified Buckingham (Exp-Six) Potential. *J. Chem. Phys.* **1954**, *22*, 169–186, DOI: 10.1063/1.1740026.

(24) Tiesinga, E.; Mohr, P. J.; Newell, D. B.; Taylor, B. N. "The 2018 CODATA Recommended Values of the Fundamental

Physical Constants" (Web Version 8.0). Database developed by J. Baker, M. Douma, and S. Kotochigova. Available at http://physics.nist.gov/constants, National Institute of Standards and Technology, Gaithersburg, MD 20899. 2019, accessed on July 8, 2019; https://physics.nist.gov/cgi-bin/cuu/Value?ep0.

(25) Mohr, P. J.; Newell, D. B.; Taylor, B. N.; Tiesinga, E. Data and analysis for the CODATA 2017 special fundamental constants adjustment. *Metrologia* **2018**, *55*, 125–146, DOI: 10.1088/1681-7575/aa99bc.

(26) Bartke, J.; Hentschke, R. Phase behavior of the Stockmayer fluid via molecular dynamics simulation. *Phys. Rev. E* **2007**, *75*, 061503, DOI: 10.1103/physreve.75.061503.

(27) Stockmayer, W. H. Second Virial Coefficients of Polar Gases. *J. Chem. Phys.* **1941**, *9*, 398–402, DOI: 10.1063/1.1750922.

(28) Buckingham, A. D.; Pople, J. A. The statistical mechanics of imperfect polar gases. Part 1.—Second virial coefficients. *Trans. Faraday Soc.* **1955**, *51*, 1173–1179, DOI: 10.1039/tf9555101173.

(29) Rowlinson, J. S. The second virial coefficients of polar gases. *Trans. Faraday Soc.* **1949**, *45*, 974–984, DOI: 10.1039/tf9494500974.

(30) Gámez, F.; Caro, C. The second virial coefficient for anisotropic square-well fluids. *J. Mol. Liq.* **2015**, *208*, 21–26, DOI: 10.1016/j.molliq.2015.04.011.

(31) Hirschfelder, J. O.; Curtiss, C. F.; Bird, R. B. *Molecular Theory of Gases and Liquids*; John Wiley and Sons, 1954.

(32) Ref. 31, Table II-A.

(33) Bell, I. H.; Alpert, B. K.; Bouck, L. ChebTools: C++11 (and Python) tools for working with Chebyshev expansions. *J. Open Source Soft.* **2018**, *3*, 569, DOI: 10.21105/joss.00569.

(34) Monchick, L.; Mason, E. A. Transport Properties of Polar Gases. *J. Chem. Phys.* **1961**, *35*, 1676–1697, DOI: 10.1063/1.1732130.

(35) Raghavachari, K.; Trucks, G. W.; Pople, J. A.; Head-Gordon, M. A fifth-order perturbation comparison of electron correlation theories. *Chem. Phys. Lett.* **1989**, *157*, 479–483, DOI: 10.1016/s0009-2614(89)87395-6.

(36) Garberoglio, G.; Jankowski, P.; Szalewicz, K.; Harvey, A. H. Fully quantum calculation of the second and third virial coefficients of water and its isotopologues from ab initio potentials. *Faraday Discuss.* **2018**, *212*, 467–497, DOI: 10.1039/C8FD00092A.

(37) Ortiz-Vega, D. O.; Hall, K. R.; Holste, J. C.; Arp, V. D.; Harvey, A. H.; Lemmon, E. W. Thermodynamic Properties for Helium-4. *J. Phys. Chem Ref. Data* **2019, To Be Submitted**,

(38) Cencek, W.; Przybytek, M.; Komasa, J.; Mehl, J. B.; Jeziorski, B.; Szalewicz, K. Effects of adiabatic, relativistic, and quantum electrodynamics interactions on the pair potential and thermophysical properties of helium. *J. Chem. Phys.* **2012**, *136*, 224303, DOI: 10.1063/1.4712218.

(39) Setzmann, U.; Wagner, W. A New Equation of State and Tables of Thermodynamic Properties for Methane Covering the Range from the Melting Line to 625 K at Pressures up to 100 MPa. *J. Phys. Chem. Ref. Data* **1991**, *20*, 1061–1155, DOI: 10.1063/1.555898.

(40) Hellmann, R.; Bich, E.; Vogel, E. Ab initio intermolecular potential energy surface and second pressure virial coefficients of methane. *J. Chem. Phys.* **2008**, *128*, 214303, DOI: 10.1063/1.2932103.

(41) Hellmann, R.; Bich, E.; Vogel, E.; Dickinson, A. S.; Vesovic, V. Calculation of the transport and relaxation properties of methane. I. Shear viscosity, viscomagnetic effects, and self-diffusion. *J. Chem. Phys.* **2008**, *129*, 064302, DOI: 10.1063/1.2958279.

(42) Hellmann, R.; Bich, E.; Vogel, E.; Dickinson, A. S.; Vesovic, V. Calculation of the transport and relaxation properties of methane. II. Thermal conductivity, thermomagnetic effects, volume viscosity, and nuclear-spin relaxation. *J. Chem. Phys.* **2009**, *130*, 124309, DOI: 10.1063/1.3098317.

(43) Wagner, W.; Pruß, A. The IAPWS Formulation 1995 for the Thermodynamic Properties of Ordinary Water Substance for General and Scientific Use. *J. Phys. Chem. Ref. Data* **2002**, *31*, 387–535, DOI: 10.1063/1.1461829.

(44) Hellmann, R.; Vogel, E. The Viscosity of Dilute Water Vapor Revisited: New Reference Values from Experiment and Theory for Temperatures between (250 and 2500) K. *J. Chem. Eng. Data* **2015**, *60*, 3600–3605, DOI: 10.1021/acs.jced.5b00599.

(45) Hellmann, R.; Bich, E. An improved kinetic theory approach for calculating the thermal conductivity of polyatomic gases. *Mol. Phys.* **2015**, *113*, 176–183, DOI: 10.1080/00268976.2014.951703.

(46) Bukowski, R.; Szalewicz, K.; Groenenboom, G. C.; van der Avoird, A. Predictions of the Properties of Water from First Principles. *Science* **2007**, *315*, 1249–1252, DOI: 10.1126/science.1136371.

(47) Bukowski, R.; Szalewicz, K.; Groenenboom, G. C.; van der Avoird, A. Polarizable interaction potential for water from coupled cluster calculations. I. Analysis of dimer potential energy surface. *J. Chem. Phys.* **2008**, *128*, 094313, DOI: 10.1063/1.2832746.

(48) Herrig, S.; Thol, M.; Harvey, A. H.; Lemmon, E. W. A Reference Equation of State for Heavy Water. *J. Phys. Chem. Ref. Data* **2018**, *47*, 043102, DOI: 10.1063/1.5053993.

(49) Hellmann, R.; Bich, E. Transport properties of dilute D_2O vapour from first principles. *Mol. Phys.* **2016**, *115*, 1057–1064, DOI: 10.1080/00268976.2016.1226443.

(50) Thol, M.; Beckmüller, R.; Weiss, R.; Harvey, A. H.; Lemmon, E. W.; Jacobsen, R. T.; Span, R. Thermodynamic Properties for Neon for Temperatures from the Triple Point to 700 K at Pressures to 700 MPa. *J. Phys. Chem Ref. Data* **2019, To Be Submitted**,

(51) Bich, E.; Hellmann, R.; Vogel, E. Erratum to : "Ab initio potential energy curve for the neon atom pair and thermophysical properties for the dilute neon gas. II. Thermophysical properties for low-density neon". *Mol. Phys.* **2008**, *106*, 1107–1122, DOI: 10.1080/00268970802302662.

(52) Span, R.; Lemmon, E. W.; Jacobsen, R. T.; Wagner, W.; Yokozeki, A. A Reference Equation of State for the Thermodynamic Properties of Nitrogen for Temperatures from 63.151 to 1000 K and Pressures to 2200 MPa. *J. Phys. Chem. Ref. Data* **2000**, *29*, 1361–1433, DOI: 10.1063/1.1349047.

(53) Hellmann, R. Ab initio potential energy surface for the nitrogen molecule pair and thermophysical properties of nitrogen gas. *Mol. Phys.* **2013**, *111*, 387–401, DOI: 10.1080/00268976.2012.726379.

(54) Bücker, D.; Wagner, W. A Reference Equation of State for the Thermodynamic Properties of Ethane for Temperatures from the Melting Line to 675 K and Pressures up to 900 MPa. *J. Phys. Chem. Ref. Data* **2006**, *35*, 205–266, DOI: 10.1063/1.1859286.

(55) Hellmann, R. Reference Values for the Second Virial Coefficient and Three Dilute

Gas Transport Properties of Ethane from a State-of-the-Art Intermolecular Potential Energy Surface. *J. Chem. Eng. Data* **2018**, *63*, 470–481, DOI: 10.1021/acs.jced.7b01069.

(56) Lemmon, E. W.; Span, R. Short Fundamental Equations of State for 20 Industrial Fluids. *J. Chem. Eng. Data* **2006**, *51*, 785–850, DOI: 10.1021/je050186n.

(57) Hellmann, R.; Bich, E.; Vogel, E.; Vesovic, V. Thermophysical Properties of Dilute Hydrogen Sulfide Gas. *J. Chem. Eng. Data* **2012**, *57*, 1312–1317, DOI: 10.1021/je3000926.

(58) Tegeler, C.; Span, R.; Wagner, W. A New Equation of State for Argon Covering the Fluid Region for Temperatures From the Melting Line to 700 K at Pressures up to 1000 MPa. *J. Phys. Chem. Ref. Data* **1999**, *28*, 779–850, DOI: 10.1063/1.556037.

(59) Vogel, E.; Jäger, B.; Hellmann, R.; Bich, E. Ab initio pair potential energy curve for the argon atom pair and thermophysical properties for the dilute argon gas. II. Thermophysical properties for low-density argon. *Mol. Phys.* **2010**, *108*, 3335–3352, DOI: 10.1080/00268976.2010.507557.

(60) Song, B.; Wang, X.; Liu, Z. Recommended gas transport properties of argon at low density using ab initio potential. *Mol. Simul.* **2015**, *42*, 9–13, DOI: 10.1080/08927022.2014.1003296.

(61) Span, R.; Wagner, W. A New Equation of State for Carbon Dioxide Covering the Fluid Region from the Triple-Point Temperature to 1100 K at Pressures up to 800 MPa. *J. Phys. Chem. Ref. Data* **1996**, *25*, 1509–1596, DOI: 10.1063/1.555991.

(62) Hellmann, R. Ab initio potential energy surface for the carbon dioxide molecule pair and thermophysical properties of dilute carbon dioxide gas. *Chem. Phys. Lett.* **2014**, *613*, 133–138, DOI: 10.1016/j.cplett.2014.08.057.

(63) Crusius, J.-P.; Hellmann, R.; Hassel, E.; Bich, E. Ab initio intermolecular potential energy surface and thermophysical properties of nitrous oxide. *J. Chem. Phys.* **2015**, *142*, 244307, DOI: 10.1063/1.4922830.

(64) Thol, M.; Rutkai, G.; Köster, A.; Kortmann, M.; Span, R.; Vrabec, J. Fundamental equation of state for ethylene oxide based on a hybrid dataset. *Chem. Eng. Sci.* **2015**, *121*, 87–99, DOI: 10.1016/j.ces.2014.07.051.

(65) Crusius, J.-P.; Hellmann, R.; Hassel, E.; Bich, E. Intermolecular potential energy surface and thermophysical properties of ethylene oxide. *J. Chem. Phys.* **2014**, *141*, 164322, DOI: 10.1063/1.4899074.

(66) Lemmon, E. W.; McLinden, M. O.; Wagner, W. Thermodynamic Properties of Propane. III. A Reference Equation of State for Temperatures from the Melting Line to 650 K and Pressures up to 1000 MPa. *J. Chem. Eng. Data* **2009**, *54*, 3141–3180, DOI: 10.1021/je900217v.

(67) Hellmann, R. Intermolecular potential energy surface and thermophysical properties of propane. *J. Chem. Phys.* **2017**, *146*, 114304, DOI: 10.1063/1.4978412.

(68) Jäger, B.; Hellmann, R.; Bich, E.; Vogel, E. State-of-the-art ab initio potential energy curve for the krypton atom pair and thermophysical properties of dilute krypton gas. *J. Chem. Phys.* **2016**, *144*, 114304, DOI: 10.1063/1.4943959.

(69) Hellmann, R.; Jäger, B.; Bich, E. State-of-the-art ab initio potential energy curve for the xenon atom pair and related spectroscopic and thermophysical properties. *J. Chem. Phys.* **2017**, *147*, 034304, DOI: 10.1063/1.4994267.

(70) Harvey, A. H.; Lemmon, E. W. Correlation for the Second Virial Coefficient of

Water. *J. Phys. Chem. Ref. Data* **2004**, *33*, 369–376, DOI: 10.1063/1.1587731.

(71) Kestin, J.; Knierim, K.; Mason, E. A.; Najafi, B.; Ro, S. T.; Waldman, M. Equilibrium and Transport Properties of the Noble Gases and Their Mixtures at Low Density. *J. Phys. Chem. Ref. Data* **1984**, *13*, 229–303, DOI: 10.1063/1.555703.

(72) Boushehri, A.; Bzowski, J.; Kestin, J.; Mason, E. A. Equilibrium and Transport Properties of Eleven Polyatomic Gases At Low Density. *J. Phys. Chem. Ref. Data* **1987**, *16*, 445–466, DOI: 10.1063/1.555800.

(73) Boushehri, A.; Bzowski, J.; Kestin, J.; Mason, E. A. Erratum: Equilibrium and Transport Properties of Eleven Polyatomic Gases at Low Density [J. Phys. Chem. Ref. Data 16, 445 (1987)]. *J. Phys. Chem. Ref. Data* **1988**, *17*, 255–255, DOI: 10.1063/1.555820.

(74) Chapman, S.; Cowling, T. G. *The Mathematical Theory of Non-uniform Gases: An Account of the Kinetic Theory of Viscosity, Thermal Conduction and Diffusion in Gases*; Cambridge University Press, 1970.

(75) Mason, E. A.; Monchick, L. Heat Conductivity of Polyatomic and Polar Gases. *J. Chem. Phys.* **1962**, *36*, 1622–1639, DOI: 10.1063/1.1732790.

(76) Bich, E.; Mehl, J. B.; Hellmann, R.; Vesovic, V. In *Experimental Thermodynamics Volume IX*; Assael, M. J., Goodwin, A. R. H., Vesovic, V., Wakeham, W. A., Eds.; The Royal Society of Chemistry: Cambridge, 2014; Chapter 7, pp 226–252, DOI: 10.1039/9781782625254-00226.

Graphical TOC Entry